

longitude using altitude. In the CAI Level 1B product, all bands are registered to 0.5 pixels selecting the nearest neighbor pixel. Level 1B+ radiance data are projected on the Mercator projection for +60 degree latitude to -60 degree latitude or polar stereographic projection for higher than +60 degree latitude of lower than -60 degree latitude. Band to band registration is not corrected in Level 1 A but corrected in Level 1 B and 1B+.

Radiometric calibration

Radiometric calibration of CAI is obtained by measuring the output of a integrated sphere maintained at JAXA. The integration sphere is calibrated with black body. Conversion function from sensor output to radiance is a liner and *Scale* and *Offset* are given by

$$Scale = \frac{Radiance_{calibration} \times integrationTime}{(DN_{calibration} - DarkLevel)}$$

$$Offset = DarkLevel .$$

where $DN_{calibration}$ is sensor output, $Radiance_{calibration}$ radiance measurements of the integration sphere, $DarkLevel$ measurements of the dark target, $integrationTime$ sensor integration time. Using *Scale* and *Offset*, sensor output is converted to radiance as

$$Radiance = \frac{Scale \times (DN - Offset)}{integrationTime} .$$

Vicarious Calibration

After launch, vicarious calibration coefficients for CAI are determined by comparing with Aqua MODIS radiance data looking at the same area at the same time. Avoiding BRDF (bidirectional reflectance distribution function) effects, MODIS sensors' radiance are converted to the radiance in the observing geometry of GOSAT using the radiative transfer theory through the aerosol and cloud optical properties. Band 2 and 3 radiances are compared with MODIS radiances through the aerosol optical thickness in dark region, and the cloud optical thickness in bright region. Band 4 are compared with MODIS radiance through the cloud particle radius. Unfortunately MODIS doesn't have 380 nm channel, band 1 radiance simulated from band 2 and 3, radiance using radiative transfer theory through aerosol optical properties. Equation of vicarious calibration is described with a liner function, and coefficients are shown in the table.

Fig. 2 is scatterplot of radiance of simulation through aerosol optical thickness from MODIS and CAI which show that CAI radiance is brighter than MODIS radiance and uneven.

Zero level correction

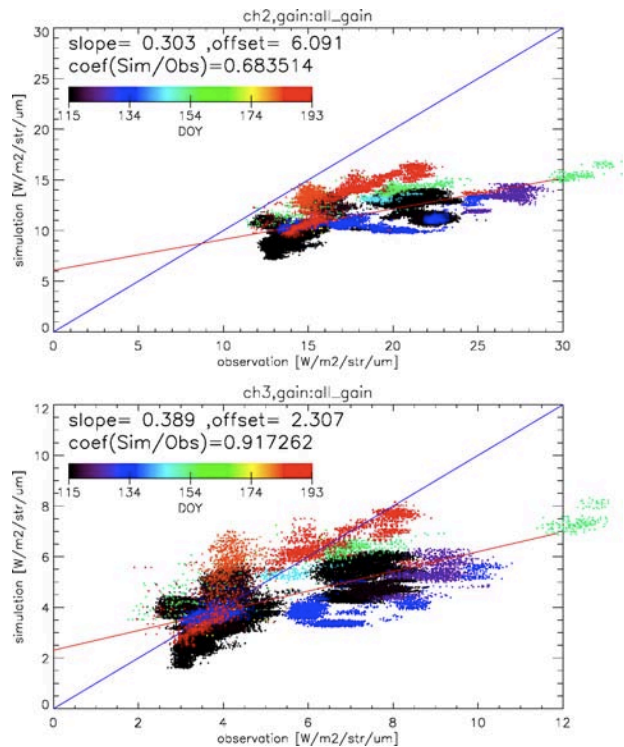


Figure 2. Scatterplot of radiance simulated from MODIS vs CAI. Upper graph is for band 2, lower graph band3.

We found a problem in CAI radiance data whose dark level are affected with incident light in the field of view. CAI L1A products has pixels in the corner of a strip where light does not reach. These pixel's value show variation proportional to the average of all pixels on the cross-track line. In figure. 3, the image above is a browse image of band 2, the graph below is sensor outputs of the band 2 corner pixels as a function of the along-track line number. Fig. 3 shows that variation of sensor output in the corner pixels is relative to brightness variation in the browse image. Due to investigation of the corner pixels, the point at problem of the dark level variability become clear. It is expected that the variation of offset of the corner pixels shows the variation of offset of the all pixels. We assumed the value of dark level of each pixel is corrected with the value of the

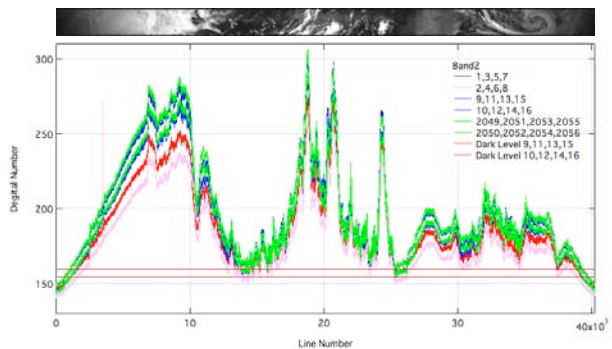


Fig. 3. Image of the measured reflectance of band 2 (above), and Sensor outputs as a function of line number (below).

corner pixels. First we have applied the correction method derived theretofore to the derivation of calibration coefficients using the integration sphere. Corrected scale is given by

$$correction_{cal} = DarkLevel_{side} - DN_{side,cal}$$

$$Scale' = \frac{Radiance_{cal} \times integrationTime}{(DN_{cal} - (DarkLevel - correction_{cal}))}$$

where DN_{side} is the average value of the corner pixels divided to odd pixels and even pixels where 4 pixels for lowest number and 4 pixels for largest number. Second the correction method is applied to the conversion equation of sensor out put to radiance. The results are given by

$$correction = DarkLevel_{side} - DN_{side}$$

$$Offset' = DarkLevel - correction$$

$$Radiance = \frac{Scale' \times (DN - Offset')}{integrationTime}$$

After applying the correction method, we have compared radiance between simulation by MODIS and CAI. Figure 4 clearly shows that scatterplot of radiance is less uneven than scatterplot presented in Fig 2. Table 2 provides a summary of the values of vicarious calibration coefficients that would be derived for each band. Figure 5 shows pseudo color images of volcanic ash clouds on Europe for 15 to 17 April 2010. On 14 April, large scale eruptions occurred in the Icelandic

Table 2. Vicarious calibration coefficients of CAI

band	slope	offset
1	1.138	0.00
2	0.946	-1.372
3	1.033	-0.189
4	1.144	0.00

volcano. On 15 April, the volcanic ash plume reached Scandinavia, CAI captured ash cloud over Germany on 16 April, ash cloud reached Russia on 17 April. CAI captured new eruption in Iceland on 17 April. These images express the feature CAI instrument is sensitive to absorption by aerosol.

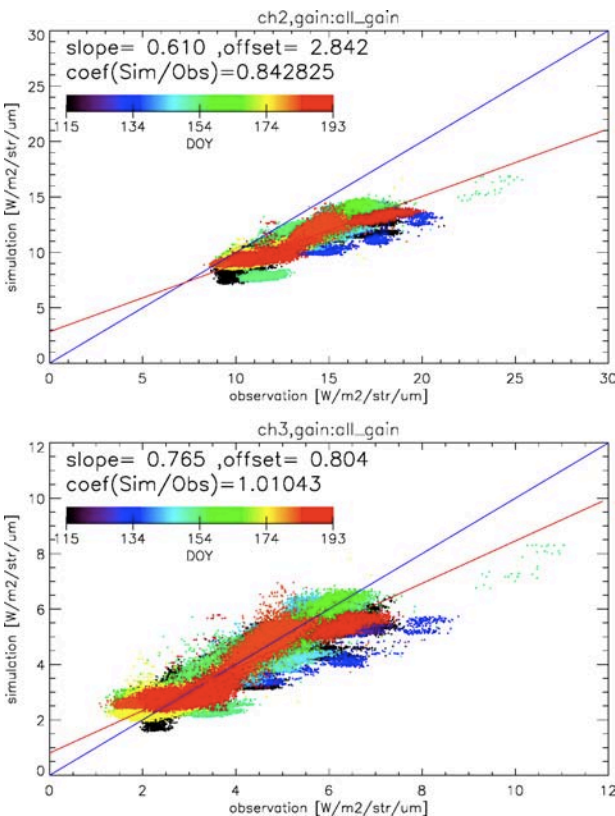


Fig. 4 Same as Fig. 2 except for dark level corrected with corner pixel values.

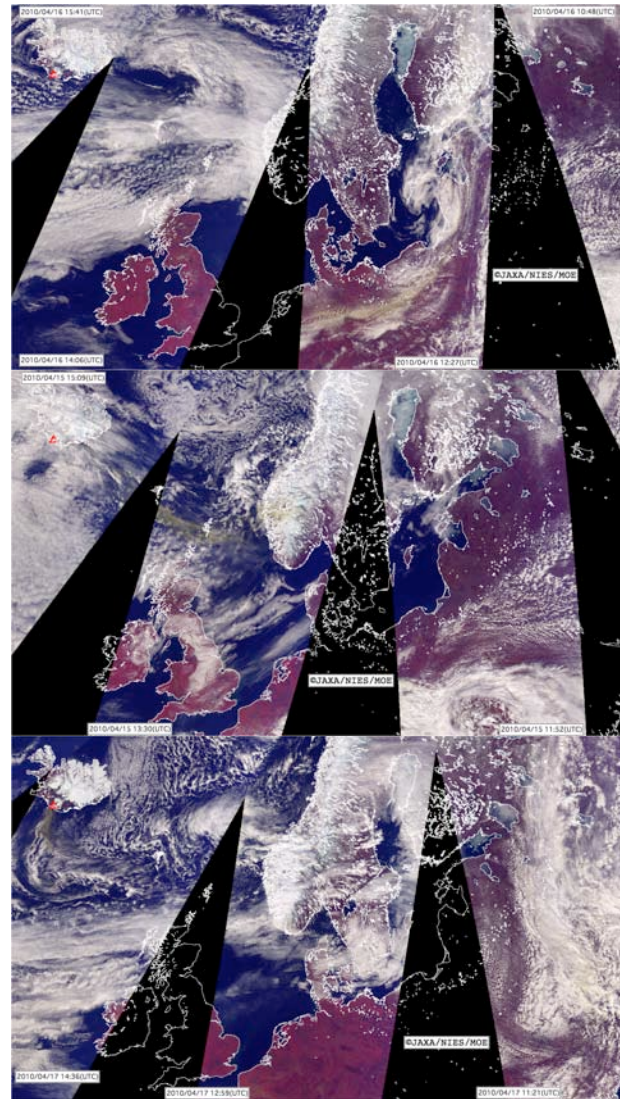


Fig. 5. CAI pseudo color images of Iceland volcanic ash cloud over Europe for 15 to 17 April. 2010. The images composed by 4 path CAI L1B data and map projected using stereograph projection. Red triangle shows Iceland volcano.

Summary

GOSAT TANSO-CAI Level 1B and Level 1B+ products are radiometrically calibrated and vicariously calibrated. We have found a problem that dark level radiance of band2 and band3 are affected with total average incident radiance. CAI band1 2 and 3 has corner pixels of cross-track line where light does not reach. Using the corner pixels' value, we can correct the dark level value of all pixels. After correction, scatterplot of radiance of MODIS simulated and CAI has become even.

References

- Kuze, Akihiko, Hiroshi Suto, Masakatsu Nakajima, and Takashi Hamazaki, 2009, Thermal and near infrared sensor for carbon observation Fourier-transform spectrometer on the Greenhouse Gases Observing Satellite for greenhouse gases monitoring, *Appl. Opt.*, 35, 6716-6733.
- Nakajima, Teruyuki, Takashi Y. Nakajima, Akiko Higurashi, Itaru Sano, Tamio Takamura, Haruma Ishida, and Nick Schutgens, 2008, A Study of Aerosol and Cloud Information Retrievals from CAI Imager on Board GOSAT Satellite, *J. Remote Sens. Soc. Jp.*, 28, 178-189.